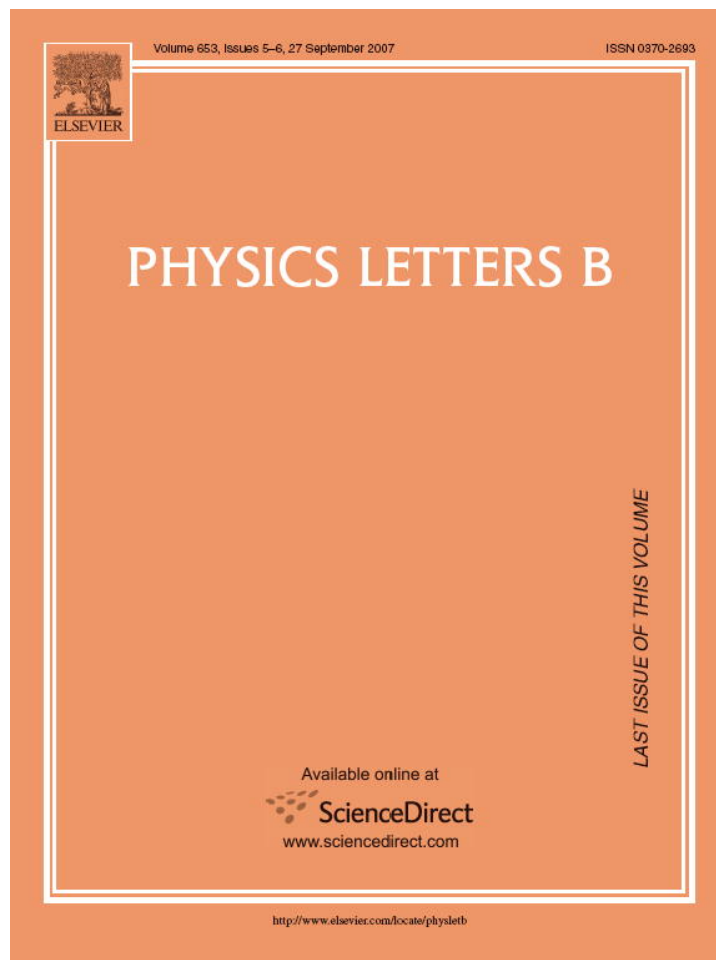


Provided for non-commercial research and education use.
Not for reproduction, distribution or commercial use.



This article was published in an Elsevier journal. The attached copy is furnished to the author for non-commercial research and education use, including for instruction at the author's institution, sharing with colleagues and providing to institution administration.

Other uses, including reproduction and distribution, or selling or licensing copies, or posting to personal, institutional or third party websites are prohibited.

In most cases authors are permitted to post their version of the article (e.g. in Word or Tex form) to their personal website or institutional repository. Authors requiring further information regarding Elsevier's archiving and manuscript policies are encouraged to visit:

<http://www.elsevier.com/copyright>



$^{16}\text{O}(e, e' p)$ reaction at large missing energy

M. Iodice^{a,*}, E. Cisbani^b, R. De Leo^c, S. Frullani^b, F. Garibaldi^b, D.L. Groep^d,
W.H.A. Hesselink^{d,e}, E. Jans^d, L. Lapikás^d, C.J.G. Onderwater^{d,e}, R. Perrino^f, J. Ryckebusch^g,
R. Starink^{d,e}, G.M. Urciuoli^h

^a INFN, Sezione Roma Tre, Via della Vasca Navale, 84, I-00146 Roma, Italy

^b INFN, Gruppo Collegato Sanità and Istituto Superiore di Sanità, Viale Regina Elena, 299, I-00161 Roma, Italy

^c University and INFN Bari, Via Amendola 173, I-70126 Bari, Italy

^d NIKHEF, PO Box 41882, 1009 DB Amsterdam, The Netherlands

^e Vrije Universiteit Amsterdam, de Boelelaan 1081, 1081 HV Amsterdam, The Netherlands

^f INFN Sezione di Lecce, via Arnesano, I-73100 Lecce, Italy

^g Department of Subatomic and Radiation Physics, Ghent University, Proeftuinstraat 86, B-9000 Gent, Belgium

^h INFN, Sezione Roma, Piazzale Aldo Moro, 2, I-00185 Roma, Italy

Received 5 March 2007; received in revised form 16 July 2007; accepted 14 August 2007

Available online 17 August 2007

Editor: D.F. Geesaman

Abstract

We investigate the origin of the strength at large missing energies in electron-induced proton knockout reactions. For that purpose the reaction $^{16}\text{O}(e, e' p)$ was studied at a central value $\omega = 215$ MeV of the energy transfer, and two values of the momentum transfer: $q = 300, 400$ MeV/ c , corresponding to the “dip region”. Differential cross sections were determined in a large range of missing energy ($E_m = 0$ –140 MeV) and proton emission angle ($\gamma_{pq} = 0$ –110°), and compared to predictions of a model that includes nucleon–nucleon short-range correlations and two-body currents. It is observed that, in the kinematic domain covered by this experiment, the largest contribution to the cross section stems from two-body currents, while short-range correlations contribute a significant fraction.

© 2007 Elsevier B.V. All rights reserved.

PACS: 21.10.Pc; 24.10.-i; 25.30.Fj

Keywords: Electron-induced knockout reactions; Short-range correlations; Two-body currents

Electron-induced proton knockout $A(e, e' p)$ reactions, at low values of missing energy E_m and missing momentum p_m , are dominated by direct processes, where the detected proton is the one that was hit by the transferred virtual photon (impulse approximation), while the recoiling ($A-1$) nucleus is left in an (excited) state, of which most properties are well described by mean-field theory. At larger E_m and p_m , other reaction mechanisms, as two- and multi-nucleon knockout, start to play a role. Here, the undetected ($A-1$) system could consist of a residual nucleus and one or more nucleons that were cor-

related with the hit nucleon and that have been knocked out in the reaction. These mechanisms should be dominant when the values of missing energy are higher than those expected from mean-field theory for the deepest bound state and where still an appreciable strength is measured (see for example [1–4] and references therein). The aim of the present Letter is to examine the origin of this excess strength in terms of short-range correlations (SRC) and two-body currents. For that purpose two channels can be studied: exclusive two-nucleon knockout or semi-inclusive one-nucleon knockout.

In the two-nucleon knockout ($e, e' pN$) reaction, SRC in nuclei are probed directly by measuring the cross section for transitions to selected states at small excitation energy in the residual nucleus [5–8]. The single-nucleon knockout ($e, e' p$)

* Corresponding author.

E-mail address: mauro.iodice@roma3.infn.it (M. Iodice).

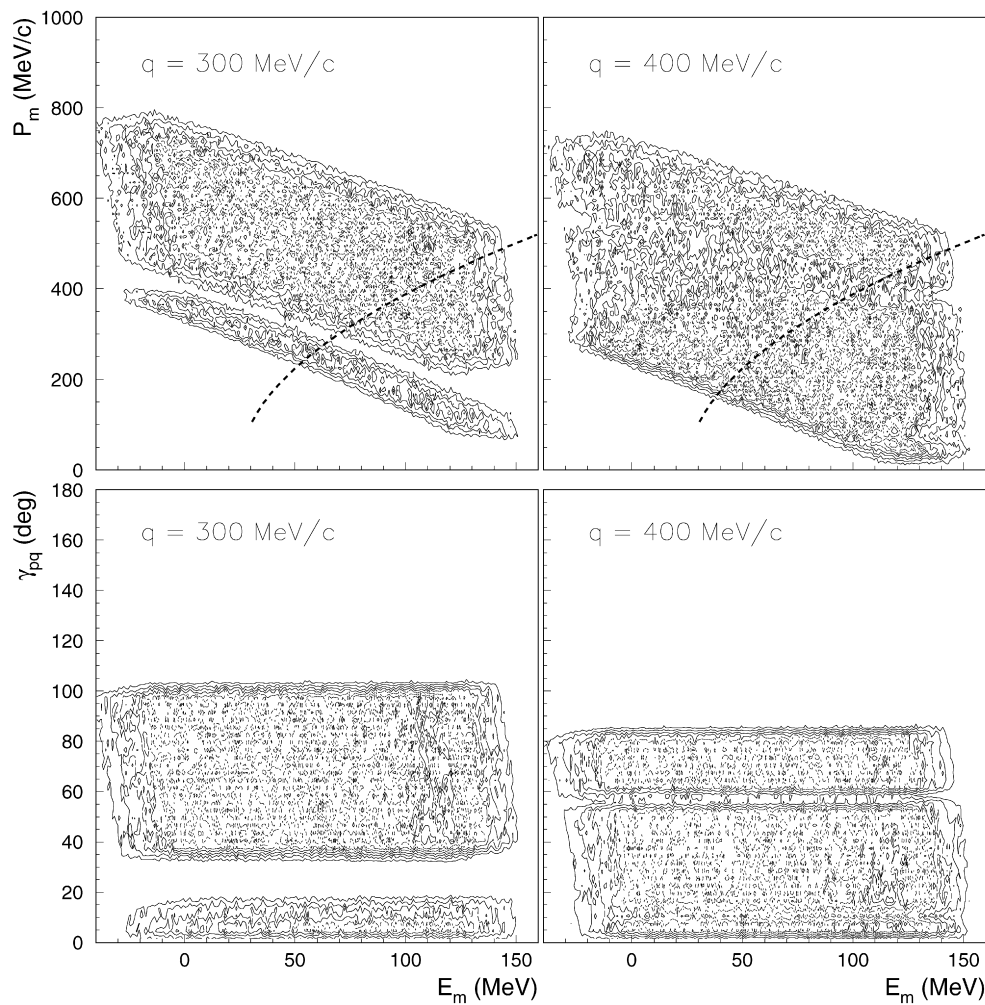


Fig. 1. Contours of the detection volumes in the (E_m, p_m) phase space (top panels) and (E_m, γ_{pq}) plane (bottom panels) for the kinematics with $q = 300$ MeV/c (left) and 400 MeV/c (right). The dashed curves show the position of the ridge according to Eq. (1).

reaction can provide information on the nucleon spectral function at large energy and momentum, which is sensitive to the nucleon–nucleon interaction at short distance (cf. Refs. [9] and [10]). However, in both cases other competing processes contribute to the cross section. In particular, two-body currents, which include meson-exchange currents (MEC) and intermediate Δ -excitation with a subsequent $\Delta N \rightarrow NN$ interaction, are known to make a substantial contribution to both the cross section of the exclusive $(e, e'pN)$ reaction and the semi-inclusive $(e, e'p)$ reaction. Hence, for these reactions a decomposition of the cross section into contributions from one-body and two-body hadronic currents can only be made by comparing the data with calculated cross sections that include both processes.

The semi-inclusive $(e, e'p)$ data have to be compared to cross sections calculated for a large domain in missing energy E_m and missing momentum p_m , because the relative contribution of either of the two processes to this reaction depends on these kinematic variables. Furthermore, in choosing the (E_m, p_m) domain for which this comparison is made, one has to take into account that in the process of interest two particles are emitted and only one is detected. Thereby, E_m and p_m are largely determined by the kinetic energy and momentum

of the undetected nucleon [11,12]. Neglecting the momentum and intrinsic excitation of the recoiling $(A-2)$ nucleus, the non-relativistic relation between these quantities reads:

$$E_m = E_{\text{thr}} + \frac{A-2}{A-1} \frac{p_m^2}{2M}, \quad (1)$$

where M is the nucleon mass, the threshold energy for two-nucleon knockout $E_{\text{thr}} = E_A - E_{(A-2)}$ is the difference between the binding energies of the A and $(A-2)$ nucleon systems, and the factor $\frac{p_m^2}{2M}$ in the second term is the kinetic energy of the undetected nucleon. This term accounts for the excitation energy of the $(A-1)$ system [13]. Eq. (1) indicates that the largest cross sections are expected along a parabolic curve in the (E_m, p_m) plane, shown in Fig. 1. The pair-momentum distribution inside the nucleus, final-state interactions and differences in intrinsic excitation of the $(A-2)$ nucleon system cause a smearing of this reaction strength. Hence, one may expect a broad ridge in the (E_m, p_m) plane, the top location of which is represented by Eq. (1). These features for semi-inclusive $(e, e'p)$ reactions at kinematic conditions that are characteristic for two-nucleon knockout, are confirmed by the (E_m, p_m) spectra measured previously for the ${}^4\text{He}(e, e'p)$ reaction at energy and momentum

transfer: $(\omega, q) = (215 \text{ MeV}, 401 \text{ MeV}/c)$ [2]. The values of (ω, q) chosen for the $^{16}\text{O}(e, e'p)$ study discussed in this Letter, are about the same as those for the ^4He experiment. This allows a comparison between both data sets, which is of interest because, in a mean-field picture, in ^4He the nucleons are knocked out of the $1s$ shell, whereas in ^{16}O knockout of nucleons from the $1p$ shell is the dominant process. A detailed comparison between the data for ^{16}O and ^4He will allow to study the mass dependence of short-range correlations in nuclei.

The experiment was performed in the EMIN (external target) hall of the Amsterdam Pulse Stretcher (AmPS) facility [14] at NIKHEF. Electrons extracted from AmPS had an energy of 575 MeV. The target used in this experiment was a single foil waterfall target [15]. A thin film of water was formed due to surface tension and adherence to two metal bars positioned below a thin slit, through which the water was pumped from a reservoir. The scattered electrons and emitted protons were detected in the QDQ high-resolution magnetic spectrometer [16] and in the large-acceptance scintillator detector HADRON3 [17], respectively. The latter detector consists of two hodoscope layers (H1 and H2) and six energy determining layers (L1–L6) of plastic scintillator slabs. It features an angular acceptance of $\pm 14^\circ$ both in the horizontal and vertical planes, and a nominal energy acceptance of 50–225 MeV. For the present experiment the low-energy threshold was raised to 65 MeV by installation of a 5 mm thick Pb-shield in front of the detector. Thus, the detector could be placed at angles as forward as 30° without being swamped by low-energy protons, while simultaneously allowing the detection of protons along the momentum transfer \mathbf{q} . The angular resolution was 0.52° both in and out of the reaction plane.

Before starting data taking the energy-response of HADRON3 was calibrated using the continuous energy-spectrum of the detected protons (singles events). The high voltages of all photo-multipliers were set such that the ADC value corresponding to the maximum energy-loss of the protons in a specific layer was about 75% of the range. The kinetic energy of the protons was determined from the amount of light measured in the layer in which the particle was stopped. This amount of light and that measured in the preceding layer were used for particle identification [17]. The arrival time of the protons in the HADRON3 detector was extracted from the signals in the first energy-determining layer. A time resolution of 700 ps (FWHM) for coincidences between electrons and protons and an overall missing energy resolution of 3.5 MeV (FWHM) were achieved.

During several dedicated runs the cross-section for elastic electron scattering off ^{16}O was measured, using events that were recorded with the QDQ magnetic spectrometer. From these data the thickness of the waterfall target was determined using the known cross section for elastic electron scattering off ^{16}O [18]. The measured thickness was $173 \pm 4 \text{ mg}/\text{cm}^2$. The error is completely dominated by the systematic experimental uncertainties. Throughout the experiment the target thickness was monitored by comparing the singles rates in the QDQ spectrometer and HADRON3 detectors. These data indicate that over the complete experiment variations in the thickness of the water film were within a range of $\pm 3\%$. The variations are known

with an accuracy of much better than 1% and accounted for in the normalisation.

Data for the $^{16}\text{O}(e, e'p)$ reaction were taken at an average transferred energy $\omega = 210 \text{ MeV}$ and at two values of the average transferred momentum q : 300 MeV/c (kinematics I) and 400 MeV/c (kinematics II). These values of (ω, q) correspond to the so-called “dip region”, the domain between the cross-section maxima for quasi-elastic scattering and Δ -production.

For each of the kinematics I and II electron–proton coincidences were measured at four angular settings θ_p of the HADRON3 detector as follows: 40° , 81° , 100° and 122° with respect to the electron beam axis for kinematics I and 40° , 60° , 81° and 110° for kinematics II. They correspond to the following ranges in the proton emission-angle $\gamma_{pq} = \theta_p - \theta_q$ with respect to the direction θ_q of the momentum-transfer vector \mathbf{q} : $0^\circ \leq \gamma_{pq} \leq 102^\circ$ for kinematics I ($q = 300 \text{ MeV}/c$, $\theta_q = 33.6^\circ$) and $0^\circ \leq \gamma_{pq} \leq 85^\circ$ for kinematics II ($q = 400 \text{ MeV}/c$, $\theta_q = 39.3^\circ$). In the lower part of Fig. 1 the contours of the detection volumes, expressed in E_m and γ_{pq} , are displayed for the two values of the transferred momenta. The upper part of Fig. 1 shows the corresponding phase-spaces in missing energy and missing momentum. They span the ranges $-20 \leq E_m \leq 150 \text{ MeV}$ and $100 \leq p_m \leq 800 \text{ MeV}/c$, respectively.

The data were corrected for radiative effects due to internal and external Bremsstrahlung as well as ionisation, using the formalism developed by Mo and Tsai [19]. The correction procedure involves both a radiative correction K_{rad} for events inside each (E_m, p_m) bin and subtraction of radiative tails σ_{rad} towards higher missing energies than the E_m bin that is actually being corrected. The shape of these tails is accurately known from QED, their amplitude depends on the cross section of the generating process.

The radiative unfolding in the two-dimensional (E_m, p_m) plane was conducted as follows. Starting at the lowest missing energy $E_m(i = 1)$, the cross sections in this column of bins $(E_m(1), p_m(j))$ were corrected for the loss of events by multiplying with $K_{\text{rad}}(1, j)$ (a typical value is 1.37), where j runs over all p_m bins in the experimental acceptance. Next, the radiative tails stemming from the column $(E_m(i = 1), p_m(j))$ were calculated and subtracted from all bins $(E_m(i' > i), p_m(j'))$ within the acceptance. The contribution of radiative tails that originate from p_m values outside the present kinematic acceptance (but radiating into it), were calculated by fitting the (smooth) p_m dependence. For the present kinematic regime no p_m bins were needed more than 40 and 60 MeV/c above the edge of the kinematic acceptances of $q = 300$ and $q = 400 \text{ MeV}/c$, respectively. This procedure was then repeated for the (corrected) strength of the second row of bins $(E_m(i = 2), p_m(j))$ and so forth. In case of a bin with a small number of events, and consequently a small statistical accuracy (typically occurring at the edges of the kinematic acceptance), we calculated the amplitude of the tails σ_{rad} from a fit to the p_m dependence surrounding that bin, instead of from its contents.

In the subtraction procedure especially the tails originating from transitions to the $1p$ valence shell in the p_m range 50–150 MeV/c were found to contribute non-negligibly. However, the knockout of $1p_{1/2}$ and $1p_{3/2}$ protons from ^{16}O is

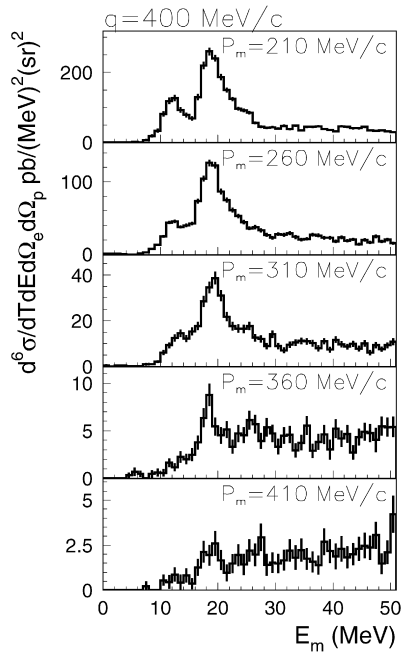


Fig. 2. Missing-energy spectra for the $^{16}\text{O}(e, e'p)$ reaction at a momentum transfer $q = 400$ MeV/c, for various values of p_m . The error bars denote statistical uncertainty only.

well known from high-resolution data previously measured at NIKHEF [20], and hence the amplitude of their radiative tails could be calculated with an accuracy of better than a few percent. For both kinematics the average relative contribution of the radiative tails σ_{rad} with respect to the uncorrected measured cross sections was 20(14)% at $p_m = 400(600)$ MeV/c in the region of $1s$ knockout ($E_m = 25\text{--}60$ MeV), and 33(18)% in the continuum region ($E_m = 60\text{--}140$ MeV).

The radiatively corrected six-fold differential cross sections, are shown in Figs. 2 and 3. The total systematic error in the cross section amounts to 7%. It results from the quadratic sum of 5% uncertainty in the radiative unfolding procedure including extrapolation of the continuum strength outside the measured region, and a 5% systematic experimental error. The latter results mainly from the uncertainties in the HADRON3 detection efficiency (3%) and in the target thickness determination (2.5%).

Fig. 2 shows the cross sections measured at a momentum transfer $q = 400$ MeV/c. They are displayed as a function of E_m in the range 0–50 MeV, at five central values of the missing momentum. It is clear that the cross section at small E_m ($10 \leq E_m \leq 20$ MeV), corresponding to knockout of a proton from the $1p$ shell and leaving the residual nucleus in a state with small excitation energy, decreases rapidly at increasing missing momentum. This trend is characteristic for the proton momentum distribution in a nucleus as calculated in a mean field approach. A similar observation has been made for the $^4\text{He}(e, e'p)$ reaction (cf. Ref. [2]). On the contrary, above $E_m \approx 25$ MeV the p_m dependence of the cross section is softer. In this domain knockout of two or more nucleons gradually becomes the dominating reaction mechanism (see Fig. 2). According to Eq. (1), the missing energy E_m and missing momentum

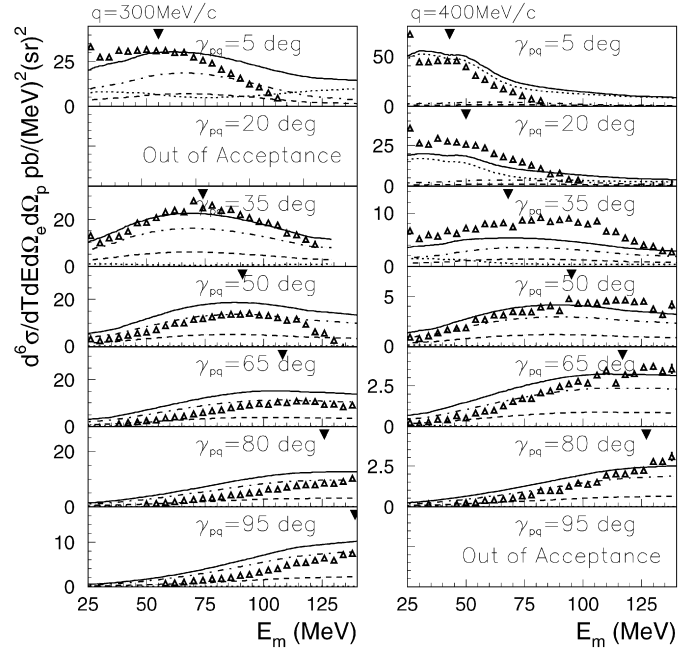


Fig. 3. Missing-energy spectra for the $^{16}\text{O}(e, e'p)$ reaction at a momentum transfer $q = 300$ MeV/c (left panel) and 400 MeV/c (right panel). The dotted curves correspond to calculated cross sections for knockout of a proton from the s -shell. The dashed (dot-dash) curves represent the results from calculations of two-nucleon knockout due to one-body (two-body) hadronic currents. The solid curve is the coherent sum of all contributions. The black upside-down triangles show the position where the maximum strength from correlated pairs is expected according to Eq. (1). For each E_m bin both the data and the curves have been integrated over the range (typically 50–100 MeV/c wide) of allowed p_m -values in the experimental phase space. The central values of these p_m ranges are (negatively) correlated with E_m .

p_m are correlated in a two-nucleon knockout reaction in which only one nucleon is detected. Indeed, the strength of the continuum cross section in Fig. 2 is seen to shift toward higher E_m with increasing p_m .

In Fig. 3 the six-fold differential cross sections for the $^{16}\text{O}(e, e'p)$ reaction measured as a function of the missing energy at $q = 300$ MeV/c (left) and 400 MeV/c (right), are presented for seven bins in γ_{pq} , together with calculated cross sections. This part of the E_m spectrum contains the information on short-range correlations and other processes that contribute to two-nucleon knockout. Two γ_{pq} domains do not contain data. They are outside the acceptance covered in the present experiment (see Fig. 1).

The theoretical cross sections for two-nucleon knockout, also shown in Fig. 3, were evaluated in an unfactorised framework based on the assumption mentioned above, i.e., that in a semi-inclusive ($e, e'p$) reaction at large E_m two nucleons are emitted, of which one is detected [9]. They include contributions of one-body as well as two-body hadronic currents, and can be considered as an extension of the two-nucleon knockout model for transitions to the ground state and states at low excitation energy in the $^{16}\text{O}(e, e'pN)$ reaction (N is either a proton or a neutron) to energies beyond the nucleon separation energy [21]. The model does not explicitly include rescattering processes of the type $^{16}\text{O}(e, e'p)$ followed by (p, Np') for ex-

ample. Detailed studies like the one reported in Ref. [22] show that the effect of the rescattering processes is relatively modest. In the representation of Fig. 3 the structure of the ridge stemming from two-nucleon knockout is most significant. The results obtained for the ${}^4\text{He}(e, e'p)$ reaction [2] were presented in the same way. Both data-sets exhibit qualitatively similar features. Note that the cross sections systematically decrease at increasing γ_{pq} and that the values of E_m at which the cross section reaches a maximum increase with increasing γ_{pq} . This is characteristic for a two-nucleon knockout reaction in which only one of the ejectiles is detected, as expressed by Eq. (1). In such a reaction the missing energy and momentum are largely accounted for by the unobserved nucleon, as indicated by the dashed curve in Fig. 1. Hence, the angles at which the cross sections reach the maximum values and the widths of the distributions are characteristic for the internal initial-state momentum of the knocked-out nucleon pair.

The various curves in Fig. 3 represent the results of un-factorised distorted-wave calculations, performed for the two values of the transferred momentum, i.e., 300 and 400 MeV/c. The dotted curve accounts for the contribution of single-proton knockout from the $1s$ shell. For $\gamma_{pq} \geq 25^\circ$ this cross section becomes negligibly small. The computed $(e, e'p)$ strength attributed to the SRC, i.e., central short-range and tensor correlations, are presented by the dashed curves. This strength is produced through the one-body currents and would vanish identically in a mean-field theory. The $(e, e'p)$ strength due to the genuine two-body currents, i.e., meson-exchange and isobar currents, are presented by the dot-dash curves. Finally, the solid curves represent the coherent sum of all contributions. It is observed that the cross sections stemming from the SRC (or, one-body currents) and those from meson-exchange and isobar currents (or, two-body currents) exhibit a similar dependence on E_m . In the considered kinematic domain the correlations (dominated by the NN tensor contribution) account for about a third of the total strength.

Comparison of the data with the calculated cross sections indicates that there is acceptable overall agreement. The calculations reasonably reproduce the dependence on E_m of the cross sections at larger values of γ_{pq} . For both kinematics I and II, the experimental cross sections decrease by large factors, in the range between three to twenty, depending on the value of γ_{pq} . This reduction would be about 30% if caused only by single-proton knockout, proportional to the proton electromagnetic form factors. As can be appreciated from Fig. 1, the data at $\gamma_{pq} = 5^\circ$ and $\gamma_{pq} = 20^\circ$ probe relatively small values of the missing momentum ($p_m < 300$ MeV/c) and receive important contributions for single-proton knockout from the $1s$ shell. From Fig. 1 it becomes clear that p_m decreases with increasing E_m . This makes the cross sections extremely sensitive to the high E_m tails of the $1s$ -strength distribution. The dotted curves in Fig. 3 are computed by evaluating the cross section for proton knockout from the $1s$ shell at various proton kinetic energies and folding the result with a model for the E_m dependence of the $1s$ strength in ${}^{15}\text{N}$. Thereby, we rely on a prescription which is due to Jeukenne and Mahaux [23,24]. From the uppermost panels ($\gamma_{pq} = 5^\circ$) in Fig. 3 it becomes

clear that this prescription overpredicts the high- E_m tail of the $1s$ strength.

In Ref. [25] the theoretical model presented here was compared to ${}^{16}\text{O}(e, e'p)$ JLAB data that cover a range of missing energies and momenta comparable to the present data. However, the JLAB data were obtained in quasi-elastic kinematics at considerably larger values of the energy and momentum transfer $(\omega, q) = (439 \text{ MeV}, 1000 \text{ MeV}/c)$. The model could account for the transverse nature and the shape of the JLAB data, but for only half of the magnitude of the measured cross sections. The very different kinematics makes a direct comparison between the model calculations for the JLAB and our data difficult. The JLAB data are obtained at considerably larger values of the four-momentum transfer than ours. Under those conditions, the SRC (or, one-body currents) gain in relative importance with respect to the two-body currents [9]. It emerges that the parameter-free model presented here can deal with the shape of the missing-energy dependence of the ${}^{16}\text{O}(e, e'p)$ cross sections, but falls short in predicting their absolute magnitude.

In Ref. [2] the ${}^4\text{He}(e, e'p)$ data taken at $\omega = 215$ MeV and $q = 401$ MeV/c are presented and compared to the results of microscopic calculations performed by Laget. The experimental and calculated cross sections presented in Fig. 3 exhibit similar features as those for the ${}^4\text{He}(e, e'p)$ reaction. Detailed comparison of the calculations for ${}^4\text{He}$ (Fig. 3 of Ref. [2]) and ${}^{16}\text{O}$ (right panels of Fig. 3 of this Letter) shows that for ${}^4\text{He}$ the inclusion of two-body currents enhances the cross sections in the top of the bump by a factor 1.5 (3) for $\gamma_{pq} = 35(90)^\circ$, whereas for ${}^{16}\text{O}$ the enhancement is a factor of about 4 to 5, independent of γ_{pq} (and hence of p_m). This indicates that the amount of available nucleon pairs and their corresponding pair quantum numbers considerably influence the relative strength of two-nucleon knockout driven by two-body currents relative to that driven by SRCs. SRCs are associated to nucleon pairs in relative S states [7,9]. A large fraction of the proton–proton and proton–neutron pairs in ${}^4\text{He}$ resides in relative S states, whereas in ${}^{16}\text{O}$ the fraction of nucleon–nucleon pairs in relative S states is smaller.

In conclusion, the comparison of the present ${}^{16}\text{O}(e, e'p)$ data with advanced model calculations shows that, at missing energies above about 25 MeV and in the studied kinematic range of missing momentum, single-proton knockout is manifestly small. In this energy region the contributions from two-body (meson-exchange and isobar) currents and to a lesser extent those from short-range correlations dominate the cross sections. In order to further distinguish between the latter two contributions in future experiments a longitudinal-transverse separation of the cross section is mandatory.

Acknowledgements

We would like to thank S. Colilli, R. Crateri, F. Giuliani, M. Gricia, M. Lucentini and F. Santavenere for the preparation and maintenance of the waterfall target.

This work is part of the research program of the Foundation for Fundamental Research of Matter (FOM), which is fi-

nancially supported by the Netherlands' Organisation for the Advancement of Pure Research (NWO).

References

- [1] C. Marchand, et al., Phys. Rev. Lett. 60 (1988) 1703;
C. Marchand, et al., Phys. Rev. Lett. 60 (1988) 2704, Erratum.
- [2] J.J. van Leeuwe, et al., Phys. Lett. B 523 (2001) 6.
- [3] F. Benmokhtar, et al., Phys. Rev. Lett. 94 (2005) 082305.
- [4] K.G. Fissum, et al., Phys. Rev. C 70 (2004) 034606.
- [5] C.J.G. Onderwater, et al., Phys. Rev. Lett. 81 (1998) 2213.
- [6] D.L. Groep, et al., Phys. Rev. Lett. 83 (1999) 5443.
- [7] R. Starink, et al., Phys. Lett. B 474 (2000) 33.
- [8] R.A. Niyazo, et al., Phys. Rev. Lett. 92 (2004) 052303.
- [9] S. Janssen, J. Ryckebusch, W. Van Nespen, D. Debruyne, Nucl. Phys. A 672 (2000) 285.
- [10] D. Rohe, et al., Phys. Rev. Lett. 93 (2004) 182501.
- [11] L. Frankfurt, M. Strikman, Phys. Rep. 76 (1981) 215.
- [12] J.M. Laget, Nucl. Phys. A 358 (1981) 275.
- [13] C. Ciofi degli Atti, S. Simula, Phys. Rev. C 53 (1996) 1689.
- [14] P.K.A. de Witt Huberts, Nucl. Phys. A 553 (1993) 845c.
- [15] F. Garibaldi, et al., Nucl. Instrum. Methods Phys. Res. A 314 (1992) 1.
- [16] C. de Vries, et al., Nucl. Instrum. Methods 223 (1984) 1.
- [17] A.R. Pellegrino, et al., Nucl. Instrum. Methods Phys. Res. A 437 (1999) 188.
- [18] H. de Vries, C.W. de Jager, C. de Vries, At. Nucl. Data Tables 36 (1987) 495.
- [19] L.W. Mo, Y.S. Tsai, Rev. Mod. Phys. 41 (1969) 205.
- [20] M. Leuschner, et al., Phys. Rev. C 49 (1994) 995.
- [21] J. Ryckebusch, W. Van Nespen, Eur. Phys. J. A 20 (2004) 435.
- [22] C. Barbieri, D. Rohe, I. Sick, L. Lapikás, Phys. Lett. B 608 (2005) 45.
- [23] J.P. Jeukenne, C. Mahaux, Nucl. Phys. A 394 (1983) 445.
- [24] J. Ryckebusch, et al., Nucl. Phys. A 624 (1997) 581.
- [25] N. Liyanage, et al., Phys. Rev. Lett. 86 (2001) 5670.